ELSEVIER

Volume 188, April 2012

CONTENTS

JOURNAL OF SOLID STATE CHEMISTRY

www.elsevier.com/locate/jssc

Abstracted/indexed in BioEngineering Abstracts, Chemical Abstracts, Coal Abstracts, Current Contents/Physics, Chemical, & Earth Sciences, Engineering Index, Research Alert, SCISEARCH, Science Abstracts, and Science Citation Index. Also covered in the abstract and citation database SciVerse SCOPUS®. Full text available on SciVerse ScienceDirect®.

Regular Articles

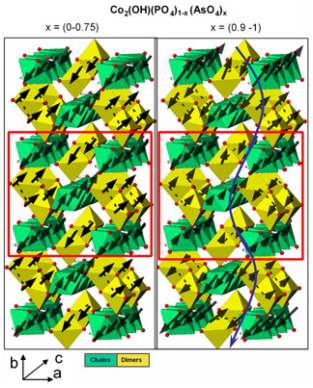

Magnetic structures of $Co_2(OH)(PO_4)_{1-x}(AsO_4)_x$ $[0 \le x \le 1]$. The ordering of the magnetic moments of Co^{2+} is in *c* direction for the two crystallographic positions (dimers and chains) in all compounds. The unit cell is surrounded by a red line.

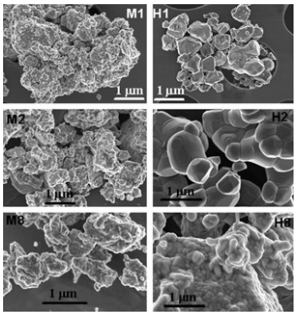

SEM micrographs corresponding to milled (**M**) and Heated (**H**) samples: $LaMnO_{3\pm\delta}$ **(M1 and H1)** $La_{0.75}Sr_{0.25}MnO_{3\pm\delta}$ **(M2** and **H2**,) and $SrMnO_{3\pm\delta}$ **(M8** and **H8)**.

Regular Articles—Continued

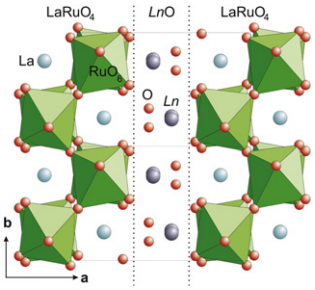

The crystal structure of $La_{2-x}Ln_xRuO_5$ (*Ln* = Pr, Nd, Sm, Gd, Dy) is shown viewed along the **c**-axis. The alternating stacking of $LaRuO_4$ and *Ln*O layers leads to the formation of zig-zag layers of corner sharing RuO_6 octahedra. The La sites in the $LaRuO_4$ layers are represented by light blue spheres, while the La/*Ln* sites in the *Ln*O layers are colored dark blue. EXAFS investigations reveal a cationic ordering with roughly 65% of the substituting *Ln* ions occupying the *Ln*O layers.

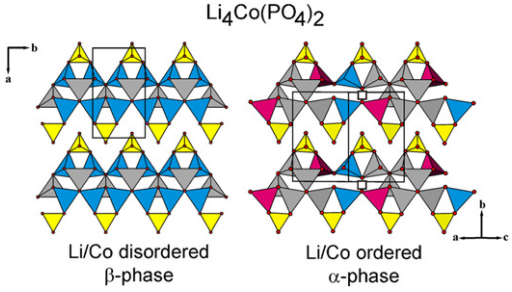

The complex formation and decomposition behavior of $Li_4Co(PO_4)_2$ with temperature has been elucidated. The crystal structure of its α-phase was determined from single crystal data, HT-XRPD allowed derivation of a structure model for the *β*-phase. Both modifications belong to the Li_3PO_4 structure family.

Continued

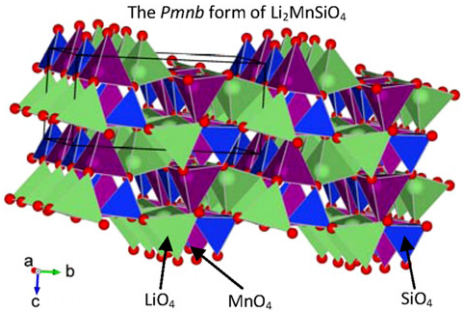

Polyhedral representation of the crystal structure of Li_2MnSiO_4 in the *Pmnb* space group. LiO_4, MnO_4 and SiO_4 tetrahedra are shown in green, purple and blue, respectively.

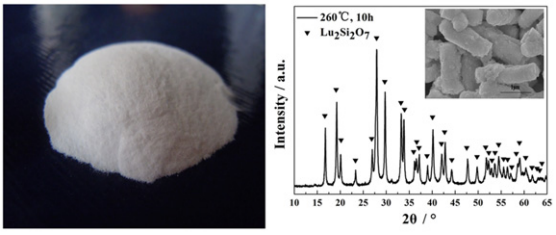

An image for the as-prepared $Lu_2Si_2O_7$ powders (left) and XRD pattern (right) (inset shows the SEM graph of powders).

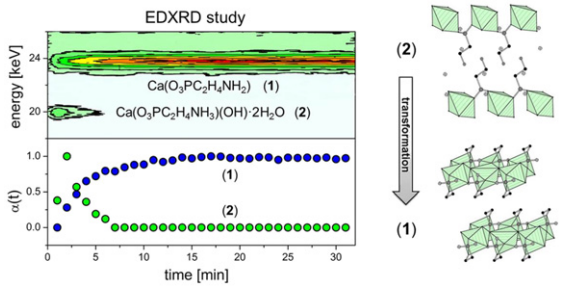

The detailed in situ energy dispersive X-ray diffraction (EDXRD) investigation on the formation of the new inorganic–organic hybrid compound $Ca(O_3PC_2H_4NH_2)$ leads to the discovery of a new crystalline intermediate phase. Both crystal structures were elucidated using X-ray powder diffraction data.

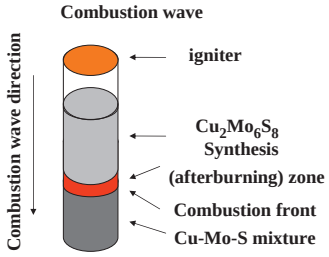

Schematic diagram of the combustion process.

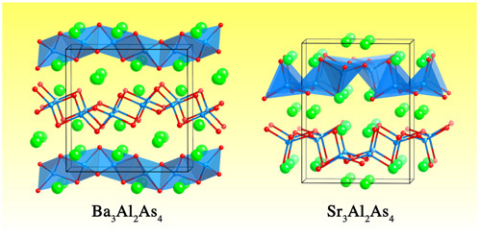

$AE_3Al_2Pn_4$ and $AE_3Ga_2Pn_4$ (AE = Ca, Sr, Ba, Eu; Pn = P, As) crystallize in two different structures—$Ca_3Al_2P_4$, $Sr_3Al_2As_4$, $Eu_3Al_2P_4$, $Eu_3Al_2As_4$, $Ca_3Ga_2P_4$, $Sr_3Ga_2P_4$, $Sr_3Ga_2As_4$, and $Eu_3Ga_2As_4$, are isotypic with the previously reported $Ca_3Al_2As_4$ (space group $C2/c$ (No. 15)), while $Ba_3Al_2P_4$ and $Ba_3Al_2As_4$ adopt a different structure known for $Na_3Fe_2S_4$ (space group *Pnma* (No. 62)). The polyanions in both structures are made up of $TrPn_4$ tetrahedra, which by sharing common corners and edges, form ${}^2_\infty[TrPn_2]^{3-}$ layers in the former and ${}^1_\infty[TrPn_2]^{3-}$ chains in $Ba_3Al_2P_4$ and $Ba_3Al_2As_4$.

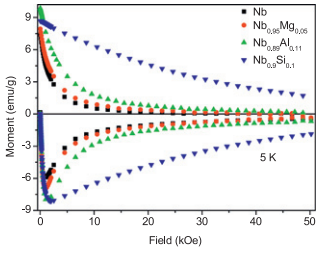

The doped Si oxide accompanied with some amount of cation vacancy in cubic NbN lattice induces relatively large magnetic hysteresis on isothermal hysteresis loops at 5 K of the dc magnetization up to 5 T among the four niobium oxynitrides containing main group elements, $Nb_{1.00}(N_{0.98}O_{0.02})$; $(Nb_{0.95}Mg_{0.05})(N_{0.92}O_{0.08})$; $(Nb_{0.89}Al_{0.11})(N_{0.84}O_{0.16})$, and $(Nb_{0.87}Si_{0.09}\square_{0.04})(N_{0.87}O_{0.13})$.

Effect of solvents on morphologies of PbTe nanostructures: Controllable synthesis of hollow and solid PbTe nanocubes by a solvothermal method
Wenzhong Wang, Lijuan Wang and Qing Zhou
page 72

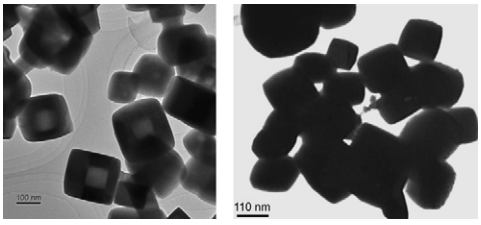

A facile solution-phase route has been developed to synthesize hollow and solid PbTe nanocubes. The possible growth mechanism of hollow and solid PbTe nanocubes was discussed in detail.

New metal-organic frameworks of $[M(C_6H_5O_7)(C_6H_6O_7)(C_6H_7O_7)(H_2O)]\cdot H_2O$ (M = La, Ce) and $[Ce_2(C_2O_4)(C_6H_6O_7)_2]\cdot 4H_2O$
Sheng-Feng Weng, Yun-Hsin Wang and Chi-Shen Lee
page 77

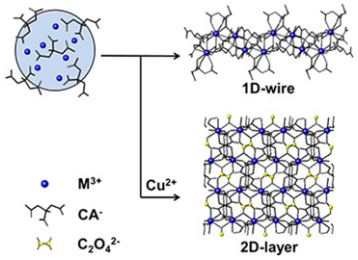

$[M(C_6H_5O_7)(C_6H_6O_7)(C_6H_7O_7)(H_2O)]\cdot H_2O$ (M = La(**1a**), Ce(**1b**)) and $[Ce_2(C_2O_4)(C_6H_6O_7)_2]\cdot 4H_2O$ (**2**)—with 1D and 2D structures were synthesized and characterized.

Thermal expansion of $Ba_2ZnSi_2O_7$, $BaZnSiO_4$ and the solid solution series $BaZn_{2-x}Mg_xSi_2O_7$ ($0 \le x \le 2$) studied by high-temperature X-ray diffraction and dilatometry
Marita Kerstan, Matthias Müller and Christian Rüssel
page 84

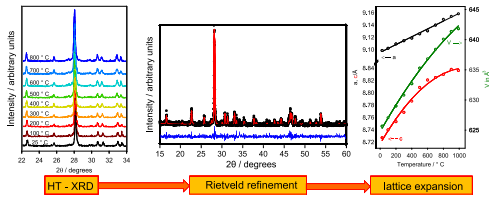

XRD-patterns of $Ba_2ZnSi_2O_7$ were recorded at different temperatures (left). For each XRD-pattern a Rietveld-refinement was performed, the image in the middle shows the XRD-pattern measured at room temperature (circles), the Rietveld calculation (red line) and the difference between them (blue line). The lattice parameters derived hereof were plottet against the temperature and fitted to a polynomial (right picture). From those polynomials the lattice expansion was calculated.

Structural variation and optical properties of $ZnO–LiGaO_2$ pseudo-binary system
Takahisa Omata, Masao Kita, Kosuke Tachibana and Shinya Otsuka-Yao-Matsuo
page 92

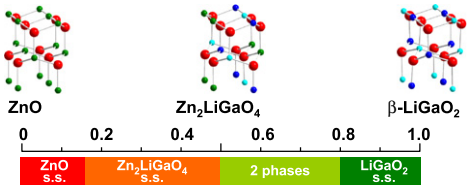

The structure of ZnO varied upon alloying with $LiGaO_2$.

Highly ordered magnetic mesoporous silicas for effective elimination of carbon monoxide
Jiho Lee and Jeong Ho Chang
page 100

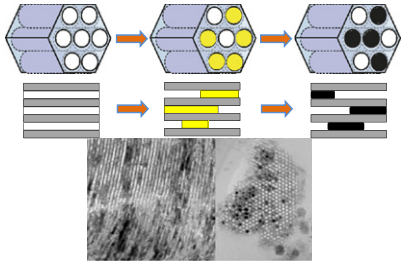

Strategy for the preparation of highly abundant Fe nanoparticle embedded MS catalyst by hydrogen reduction process and HR-TEM images of cross-sectional and top view.

Luminescence of the elpasolite series $M^I_2M^{II}MCl_6$ (M^I = Cs, Rb; M^{II} = Li, Na; M = Lu, Y, Sc, In) doped with europium using synchrotron radiation excitation
Peter A. Tanner, Chang-Kui Duan, Guohua Jia and Bing-Ming Cheng
page 105

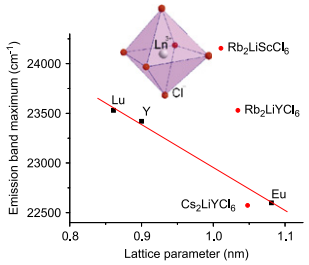

Luminescence of Eu^{3+} and Eu^{2+} in elpasolite hosts under synchrotron radiation is observed and assigned.

Continued

Corrigendum

Corrigendum to "Oxygen excess in the "114" cobaltite hexagonal structure: The ferrimagnet $CaBaCo_4O_{7.50}$" [J. Solid State Chem. 184 (2011) 2588–2594]

V. Pralong, V. Caignaert, T. Sarkar, O.I. Lebedev, V. Duffor and B. Raveau

page 109